Crystal structure of *Staphylococcus aureus* tyrosyl-tRNA synthetase in complex with a class of potent and specific inhibitors

XIAYANG QIU,[1] CHERYL A. JANSON,[1] WARD W. SMITH,[1] SUSAN M. GREEN,[1] PATRICK MCDEVITT,[1] KYUNG JOHANSON,[1] PAUL CARTER,[2] MARTIN HIBBS,[2] CERI LEWIS,[2] ALISON CHALKER,[1] ANDREW FOSBERRY,[2] JUDITH LALONDE,[1] JOHN BERGE,[2] PAMELA BROWN,[2] CATHERINE S.V. HOUGE-FRYDRYCH,[2] AND RICHARD L. JARVEST,[2]

[1]GlaxoSmithKline, King of Prussia, Pennsylvania 19406, USA
[2]GlaxoSmithKline, Harlow, Essex CM19 5AW, UK

(RECEIVED May 16, 2001; FINAL REVISION July 5, 2001; ACCEPTED July 12, 2001)

Abstract

SB-219383 and its analogues are a class of potent and specific inhibitors of bacterial tyrosyl-tRNA synthetases. Crystal structures of these inhibitors have been solved in complex with the tyrosyl-tRNA synthetase from *Staphylococcus aureus*, the bacterium that is largely responsible for hospital-acquired infections. The full-length enzyme yielded crystals that diffracted to 2.8 Å resolution, but a truncated version of the enzyme allowed the resolution to be extended to 2.2 Å. These inhibitors not only occupy the known substrate binding sites in unique ways, but also reveal a butyl binding pocket. It was reported that the *Bacillus stearothermophilus* TyrRS T51P mutant has much increased catalytic activity. The *S. aureus* enzyme happens to have a proline at position 51. Therefore, our structures may contribute to the understanding of the catalytic mechanism and provide the structural basis for designing novel antimicrobial agents.

Keywords: Tyrosyl-tRNA synthase; structure-based drug design; truncation; *Staphylococcus aureus*

Aminoacyl-tRNA synthetases play an essential role in protein synthesis by producing charged tRNAs. An amino acid is first condensed with an ATP molecule to form a stable aminoacyl-adenylate intermediate and is then transferred onto a cognate tRNA to form the desired product (Fersht 1985). Because the synthetases play such an essential role, compounds that inhibit bacterial aminoacyl-tRNA synthetases specifically could become potent antibacterial drugs (Schimmel et al. 1998). This concept is proven by the success of the broad-spectrum antibacterial drug mupirocin, which targets bacterial isoleucyl-tRNA synthetases (Hudson 1994). Multi-drug-resistant bacteria are becoming ever more prevalent and present a major threat to public health. For instance, multiple-resistant *Staphylococcus aureus* causes serious hospital-acquired infections that are very difficult to treat. With today's technology, it is possible to obtain large amounts of various aminoacyl-tRNA synthetases, especially those from virulent strains such as *S. aureus*, and use them to generate inhibitors via high-throughput screening of compound libraries. Studying aminoacyl-tRNA synthetases will not only enrich our fundamental understanding of this class of essential enzymes, but also help to combat bacterial infections.

Structural and sequence characteristics divide the various synthetases for charging the twenty different amino acids

Reprint requests to: Xiayang Qiu, Mail Code UE0447, GlaxoSmithKline, King of Prussia, Pennsylvania 19406, USA; e-mail: xiayang_qiu1@sbphrd.com; fax: (610) 270–4091.

Abbreviations: TyrRS, tyrosyl-tRNA synthetase; bsTyrRS, *Bacillus stearothermophilus* TyrRS; YRS, *Staphylococcus aureus* tyrosyl-tRNA synthetase; YRS^{tr}, C-terminal domain truncated YRS; $bsTyrRS^{tr}$, C-terminal domain truncated bsTyrRS.

Article and publication are at http://www.proteinscience.org/cgi/doi/10.1101/ps.18001.

into two classes (Eriani et al 1990). Tyrosyl-tRNA synthetase (TyrRS) belongs to the class I synthetases, characterized by a Rossmann fold in the catalytic domain and the so-called HIGH and KMSKS motifs (Eriani et al. 1990) for ATP binding. TyrRS has been studied extensively by an incredible array of biochemical techniques, which have produced some classic literature in the study of enzymatic functions (Fersht 1985). Initial crystallographic studies of *Bacillus stearothermophilus* TyrRS (bsTyrRS) were reported as early as 1973 (Reid et al. 1973), and refined X-ray crystal structures have been published, including apo bsTyrRS, bsTyrRS mutants, and bsTyrRS in complexes with tyrosine, tyrosyl-adenylate or tyrosinyl-adenylate (Brick and Blow 1987; Brown et al. 1987; Brick et al. 1989). bsTyrRS is known to act as a 94 kDa homodimer in solution (Fersht 1975). Crystal structures show that the bsTyrRS can be divided into an N-terminal α/β domain (residues 1–220), a linker peptide (residues 221–247), an α-helical domain (residues 248–319), and a C-terminal domain that is largely disordered in the bsTyrRS crystals (residues 320–419). The α-helical domain contains five helices and may contribute to tRNA binding. The α/β domain contains a six-stranded parallel β-sheet and a deep active site cleft that binds ligands such as tyrosine. The tyrosine amino group forms hydrogen bonds with Tyr169 OH, Asp78 OD1 and Gln173 OE1, the phenolic hydroxyl group forms hydrogen bonds with Asp176 OD1 and Tyr34 OH, and the carboxyl group interacts with Lys82 side chain via a water molecule (Brick and Blow 1987). All these polar interactions are well conserved in the tyrosyl- and tyrosinyl-adenylate complexes (Brick et al. 1989). In the adenylate complexes, the α-phosphate group interacts with Asp38 N, the 2′-hydroxyl group of ribose interacts with the Asp194 carboxylate and Gly192 N, the 3′-hydroxyl group interacts with a tightly bound water, while the adenine moiety makes non-polar contacts with the enzyme at Leu222, Val223, and Gly47, which are part of the HIGH motif. It has been postulated that Thr40 and His45 (part of the HIGH motif) interact with the γ-phosphate of ATP and are essential for the formation of tyrosyl-AMP (Leatherbarrow et al. 1985).

Here we report the crystal structures of the *Staphylococcus aureus* tyrosyl-tRNA synthetase (YRS) in complex with four inhibitors (Table 1). SB-219383 (Fig. 1) is a potent and specific bacterial TyrRS inhibitor originally isolated from the fermentation broth of *Micromonospora* sp. (Berge et al. 2000a ; Houge-Frydrych et al. 2000; Stefanska et al. 2000). To simplify its chemical structure, the bicyclic ring of SB219383 was cleaved to yield SB-239629 (Fig. 1), which retains potent TyrRS inhibition (Berge et al. 2000b). The addition of a butyl ester group to SB-239629 led to SB-243545 (Fig. 1) and a gain of an order of magnitude in potency (Berge et al. 2000b). SB-284485 (Fig. 1) achieved another level of chemical simplification without losing inhibitory activity (Brown et al. 2001), thus providing an excellent template for future design of TyrRS inhibitors. While three of the structures using the full-length YRS have been determined at adequate but modest resolutions (3.2 to 2.8 Å), a truncation mutant of the enzyme allowed us to extend the resolution of the fourth structure to 2.2 Å. These structures not only provide a 3-dimensional template of the enzyme from a medically important bacterial species, but also offer a practical strategy for inhibition by revealing the structural basis of binding for this class of potent and specific TyrRS inhibitors. This report should contribute to our understanding of aminoacyl-tRNA synthetases and provide valuable insights into the structure-based design of novel antimicrobial compounds.

Results and Discussion

Structure of YRS

The amino acid sequences of *S. aureus* TyrRS (YRS) and *Bacillus stearothermophilus* TyrRS (bsTyrRS) are 61% identical (Fig. 2A). Only one loop, located between helix H5 and strand D, has a difference of one residue in length between the two enzymes. Therefore, the structure of YRS is expected and proved to be similar to that of bsTyrRS. In this report, the bsTyrRS numbering system is adopted for YRS to minimize confusion. Like bsTyrRS, YRS also contains three domains. The N-terminal α/β domain (0–220) and the α-helical domain (248–323) are connected via a linker peptide (221–247), while the C-terminal domain (324–421) is disordered in the crystal (Fig. 2B). The relative orientations between the N-terminal and α-helical domains are not identical in the two enzymes, but are well within the range of variabilities in bsTyrRS structures (Brick and Blow 1987; Brick et al. 1989). There are two more residues at the YRS N-terminus, but they are away from the active site and unlikely to have any functional significance. Five additional residues are visible at the end of the YRS α-helical domain, which defined a longer helix H5′ and a slightly larger α-helical domain in YRS. There are other differences in the sizes of the secondary structures as well (Fig. 2A), caused by minor shifts of the corresponding residues. The root-mean-square (rms) difference between the YRS^{tr} and $bsTyrRS^{tr}$ structures is 1.1 Å for all α-carbon atoms. In comparison, this value is about 0.7 Å between each pair of our YRS structures. The six-stranded β-sheet in the α/β domain overlays the best, with an rms difference of only 0.37 Å between the Cα atoms of YRS and bsTyrRS. Some of the internal helices also match well, but those on the surface may differ by about 2 Å at the Cα level. The loop between helix H5 and strand D, residues 106–118, shows a shift of as much as 7 Å for Cα positions. This loop is one residue shorter in YRS, is involved in crystal packing interactions with a neighboring molecule and is known to be flexible in bsTyrRS (Brick and Blow 1987).

Table 1. *Diffraction data and structural refinement statistics*

	YRS383	YRS629	YRS545	YRS^{tr}485
Crystal				
Protein	YRS	YRS	YRS	YRS^{tr}
Inhibitor	SB-219383	SB-239629	SB-243545	SB-284485
Spacegroup	$C222_1$	$C222_1I2_12_12_1$	$I2_12_12_1$	$I2_12_12_1$
Unit cell a (Å)	71.6	70.1	66.3	66.0
b (Å)	98.5	98.9	105.8	102.9
c (Å)	142.1	143.1	140.0	139.8
Diffraction Data				
Resolution (Å)	27.0–3.2	21.0–3.2	20.0–2.8	45.0–2.2
Mosaicity (°)	0.6	0.6	0.6	1.2
No. of observations	31808	24334	18549	83183
No. of unique reflections	8530	8399	9301	23968
Redundancy	4	3	2	3
Complete % (last shell)	99 (99)	99 (99)	83 (77)	97 (69)
I/σ(I) (last shell)	7.9 (1.9)	7.1 (1.5)	7.0 (1.8)	16.9 (3.3)
R_{merge} % (last shell)[†]	12.2 (29.6)	10.8 (28.8)	10.1 (28.1)	6.6 (14.9)
Structural Refinement				
Program	XPLOR	XPLOR	XPLOR	CNX
Resolution (Å)	8.0–3.2	8.0–3.2	8.0–2.8	45.0–2.2
No. of reflections	7179	6275	8893	23342
Data cutoff (σ)	2.0	2.0	2.0	0
No. of protein atoms	2557	2557	2557	2574
No. of waters	0	0	13	190
R-factor[§]	0.269	0.257	0.205	0.183
R_{free}[¶]	0.335	0.305	0.305	0.221
Quality Indicators				
RMS bonds (Å)	0.010	0.010	0.014	0.011
RMS angles (°)	1.9	1.9	2.1	1.5
Average B factors (Å^2)	15	15	14	43
RMS B-main chain	—	—	1.9	0.9
RMS B-side chain	—	—	2.9	2.0
Ramachandran plot (%)				
most favored	77.4	78.9	88.9	93.6
generously allowed[†]	3.2	1.1	1.4	0.0
disallowed	0.0	0.0	0.0	0.0

[†] $R_{merge} = \Sigma |I - \langle I \rangle| / \Sigma I$, where I is the intensity of an observed reflection and $\langle I \rangle$ is the average intensity of multiple observations. [§] $R = \Sigma||F^{obs}| - |F^{cal}||/\Sigma|F^{obs}|$. [¶] $R_{free} = \Sigma||F^{obs}| - |F^{cal}||/\Sigma|F^{obs}|$, where F^{obs} is from a test set of reflections (5% of the total) that are not used in structural refinement. RMS, root-mean-squares.

The sequences of residues that are known to hydrogen-bond directly with tyrosine or tyrosyl adenylate (Brick and Blow 1987; Brick et al. 1989) are all conserved between the two enzymes. Still, there are a few interesting differences between theYRS and bsTyrRS active sites. In bsTyrRS the side chain of Thr51 approaches the ribose O4′ atom of tyrosyl adenylate, but the distance (3.6 Å) is too far to be considered as a hydrogen bond. This Thr51 becomes a proline in YRS (Fig. 2A). It was reported that the T51P mutant of bsTyrRS is 25-fold more active than the wild-type enzyme, possibly because of the lack of an unfavorable solvent displacement event in the mutant protein (Brown et al. 1987). In the overlay of the bsTyrRS-adenylate and YRS^{tr}485 complex structures, the Cα positions of residues 45–53 differ by an average of 0.6 Å. This small difference seems to have little to do with the T51P mutation, but rather with the A50L, I52F, and F37A differences in the vicinity (Fig. 3). In the same overlay, it appears that the adenine moiety of tyrosyl-adenylate may form good van der Waals interactions with the CD and CG atoms of the Pro51 side chain (~3.6 Å), which could be another way to explain the increased catalytic activity of the bsTyrRS T51P mutant. It is interesting to note that the Cα structures of the Lys82-Arg86 loop diverge by about 1.5 Å in the two enzymes. The structures of the linker domain, which contains Lys230 and Lys233, also vary by nearly as much. The side chain of Lys82 is known to bind the tyrosine substrate. Moreover, both the Lys82–Arg86 and Lys230–Lys233 loops are positively charged, are on the rims of the active site pocket, and could be important for TyrRS catalysis (Fersht et al. 1988) through ATP and tRNA binding. Because the former loop is in direct contact with helix H9, which is part of the TyrRS

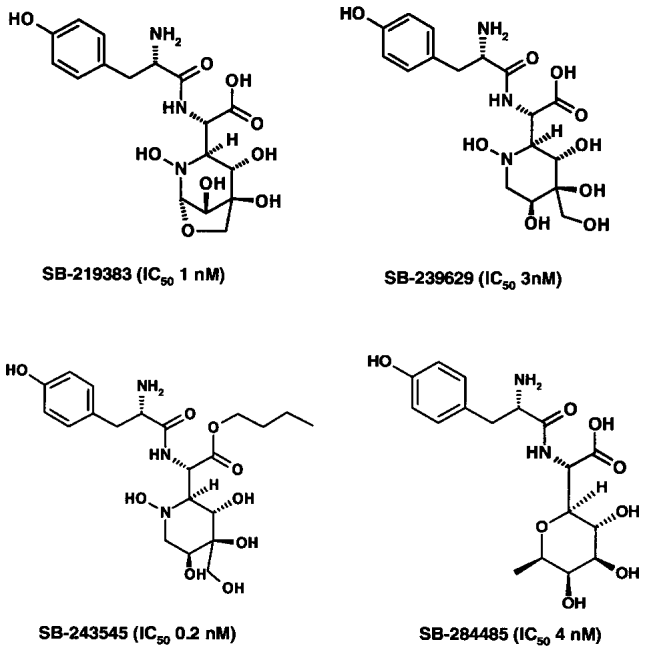

Fig. 1. Chemical structures of the *S. aureus* tyrosyl-tRNA synthetase (YRS) inhibitors. The IC_{50} values shown in this figure are cited from published reports, which were resolved by a full aminoacylation assay (Brown et al. 1999).

dimer interface, the flexibility of the Lys82–Arg86 loop may also be a way of communication between the two monomers within the TyrRS dimers.

Binding of SB-219383

SB-219383 is a potent and selective inhibitor of bacterial TyrRS, originally identified by high-throughput screening of natural products (Berge et al. 2000a; Houge-Frydrych et al. 2000; Stefanska et al. 2000). The inhibitor may be viewed as a 'dipeptide' composed of a tyrosine and an amino acid with an unusual bicyclic side chain (Fig. 1). The inhibitor has an IC_{50} of about 1 nM (Stefanska et al. 2000), which is much tighter than tyrosine (k_d ~12 μM) (Brick and Blow 1987) and the tyrosinyl adenylate analog (IC_{50} 11 nM) (Brown et al. 1999). Therefore, the binding mode of the bicyclic ring should be particularly interesting. The tyrosine-binding mode is nearly identical in all of our YRS complex structures and has been described in great length in bsTyrRS. In this section, we will focus on the binding mode of the bicyclic ring.

As shown in Figure 4, the bicyclic ring of SB-219383 forms good interactions with the protein, occupying the general region of the YRS ribose binding site. There are a total of four hydrogen bonds, involving three of the four hydroxyl groups of the bicyclic ring. The pair of hydrogen bonds to the Asp194 side chain is reminiscent of those involving the 2′-OH of ribose in the bsTyrRS–adenylate complex (Brick et al. 1989). The hydrogen bonds to the His48 side chain and to Gly36 O, on the other hand, are unique to the YRS383 complex. The bicyclic ring also forms numerous van der Waals interactions to Cys35, His48, Pro51, Gly192, and Gln195. The nitrogen atom in the bicyclic ring does not seem to be involved directly in any hydrogen bonding interactions. Moreover, the bridging methoxy moiety does not hydrogen bond with any YRS residues, indicating that the bicyclic ring may be reduced to a monocyclic six-membered ring without a significant loss in activity. This is an important issue because such a derivative compound would be much more amenable to total chemical synthesis and subsequent structure-activity relationship (SAR).

Binding of SB-239629

The monocyclic SB-239629 was derived by cleaving the bicyclic ring of SB-219383. This inhibitor has an IC_{50} of 3 nM (Berge et al. 2000b), which is not significantly different from that of SB-219383. Its mode of YRS binding is also nearly identical to that of its bicyclic parent (Fig. 5). In fact, all four hydrogen bonds observed in the YRS383 complex (Fig. 4) are conserved in the YRS629 structure. The hydroxymethyl group in SB-239629, although potentially a proton donor, is not involved in hydrogen bond interactions, but rather forms van der Waals contacts with the His48 side chain. Clearly, the YRS629 structure has demonstrated that the bicyclic ring of SB-219383 can be reduced to a monocyclic ring without altering the inhibitor binding mode.

Binding of SB-243545

SB-243545 is a butyl ester derivative of SB-239629 (Fig. 1) and binds YRS an order of magnitude more tightly than SB-239629 (Berge et al. 2000b). Although the YRS545 structure is determined in a crystal form different from that of YRS629 (Table 1), the YRS active site residues overlay well between the two structures. The tyrosyl moiety and the monocyclic side chain also bind similarly in the YRS545 and YRS629 complexes. The addition of the butyl group for SB-243545, on the other hand, reveals a novel binding pocket in YRS. This pocket is delineated by residues Ala37, Asp38, Thr40, Ala41, Ser43, Leu44, His48, and Ile101 (Fig. 6). Within the pocket, the butyl moiety forms good van der Waals interactions with Asp38, Leu44, His48, and Ile101. Except for an A37F difference between YRS and bsTyrRS (Fig. 3), the identities of the aforementioned residues are conserved in the two bacterial TyrRSs. Most of these residues superimpose well in the presence and absence of the butyl group. However, the side chain of His48 in the YRS545 structure is shifted by about 2 Å to accommodate the bound butyl group. As a result, the entire HIGH motif

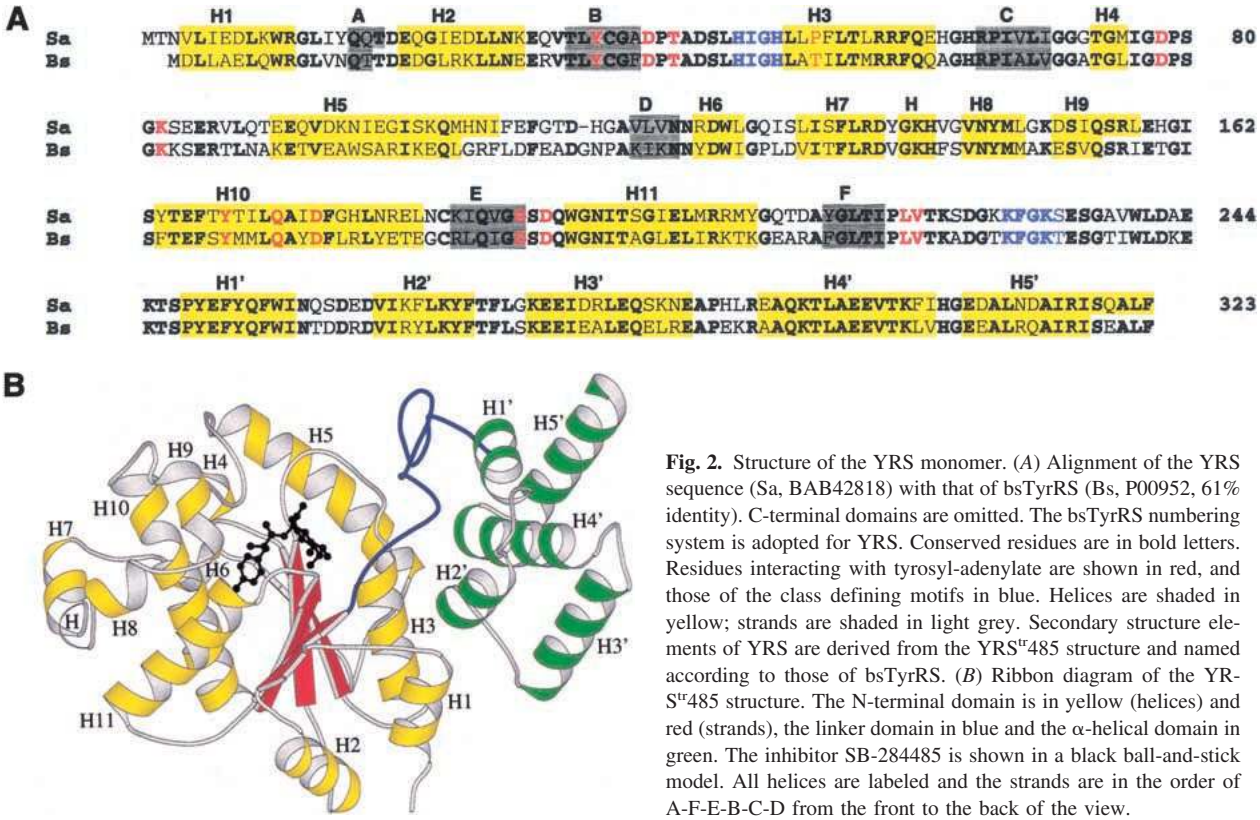

Fig. 2. Structure of the YRS monomer. (*A*) Alignment of the YRS sequence (Sa, BAB42818) with that of bsTyrRS (Bs, P00952, 61% identity). C-terminal domains are omitted. The bsTyrRS numbering system is adopted for YRS. Conserved residues are in bold letters. Residues interacting with tyrosyl-adenylate are shown in red, and those of the class defining motifs in blue. Helices are shaded in yellow; strands are shaded in light grey. Secondary structure elements of YRS are derived from the YRS^{tr}485 structure and named according to those of bsTyrRS. (*B*) Ribbon diagram of the YRS^{tr}485 structure. The N-terminal domain is in yellow (helices) and red (strands), the linker domain in blue and the α-helical domain in green. The inhibitor SB-284485 is shown in a black ball-and-stick model. All helices are labeled and the strands are in the order of A-F-E-B-C-D from the front to the back of the view.

(His45–His48) moves away from the active site (Fig. 6). Gly232–Ala238 of the linker domain (221–247) forms a β-hairpin loop that contains part of the KFGKS motif of YRS. The hairpin loop, in direct contact with the mobile HIGH motif, also shifts by greater than 2 Å (Cα) in the YRS545 structure. The changes of the HIGH and Gly232-Ala238 loops are also observed when the YRS545 and YRS^{tr}485 structures are superimposed. Because these two structures are determined in the same crystal form (Table 1), crystal packing is unlikely the cause of structural movements. The flexibility in the HIGH motif and the linker domain (221–247) may be required to support their potential roles in the transition states of the TyrRS reaction (Leatherbarrow et al. 1985). Above the butyl binding pocket, there seems to be more room for the binding of

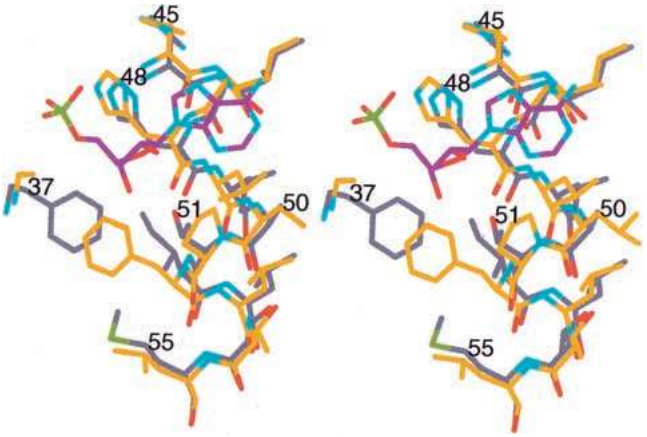

Fig. 3. Stereoview of the differences in the vicinity of the T51P mutation. Carbon atoms of YRS are in yellow, those of bsTyrRS in grey, and those of tyrosyl-adenylate (as observed in its complex with bsTyrRS) in purple. Colors of the other atoms are: oxygen–red, nitrogen–cyan, sulfur/phosphorous–green. The tyrosyl group of the tyrosyl-adenylate is omitted in this figure for clarity.

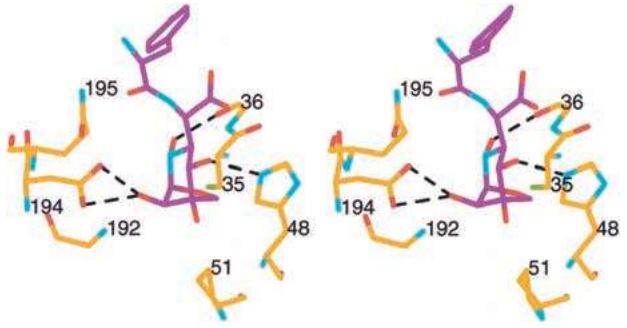

Fig. 4. Stereoview of the interactions involving the bicyclic ring of SB-219383. The inhibitor carbon atoms are drawn in purple and the YRS carbon atoms are shown in yellow. Colors of the other atoms are: oxygen–red, nitrogen–cyan, sulfur/phosphorous–green. Hydrogen bonds are illustrated by dashed lines.

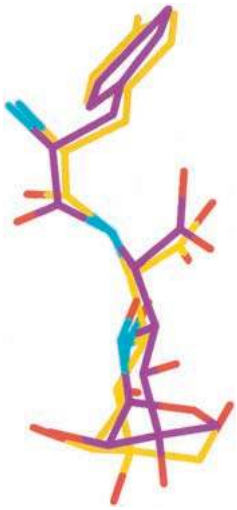

Fig. 5. The superposition of SB-239629 and SB-219383 in their complexes with YRS. The former inhibitor is shown in yellow, while the latter is in purple. This view is similar to that of Figure 4.

additional apolar or even polar substituents. It has been postulated that the ATP pyrophosphate binds in the general region between Thr40 and His45 in bsTyrRS (Leatherbarrow et al. 1985), which would project the pyrophosphate binding site just above the observed butyl binding pocket in YRS. The apolar nature of the butyl interactions suggests that the butyl pocket is not designed for pyrophosphate binding. The butyl pocket is oriented opposite to the direction which usually accommodates the $tRNA^{tyr}$ acceptor stem of class I synthetases, although the structure of a TyrRS-$tRNA^{tyr}$ complex is still to be reported. The existence of this pocket could also be completely coincidental.

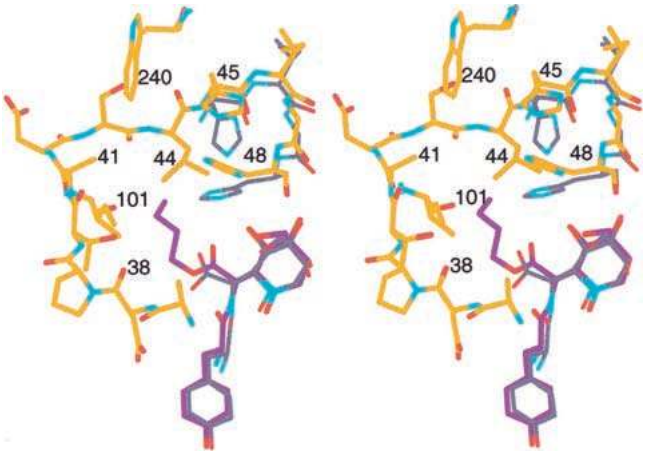

Fig. 6. Stereoview of the SB-243545 butyl binding pocket in YRS. Protein carbon atoms in the YRS545 structure are shown in yellow, while those of SB-243545 are shown in purple. The carbon atoms in the YRS629 structure are drawn in thinner grey lines. Oxygen is red and nitrogen is cyan.

Binding of SB-284485

The bicyclic side chain of SB-219383 is replaced by a fucose moiety in SB-284485, which retains potent binding (IC_{50} 4 nM) and can be synthesized readily (Brown et al. 2001). The inhibitor in complex with the C-terminal domain-truncated *S. aureus* protein yields crystals that diffract to 2.2 Å resolution, which allows us to analyze detailed interactions with more confidence. The tyrosyl group of SB-284485 forms five hydrogen bonds with YRS (Fig. 7A).

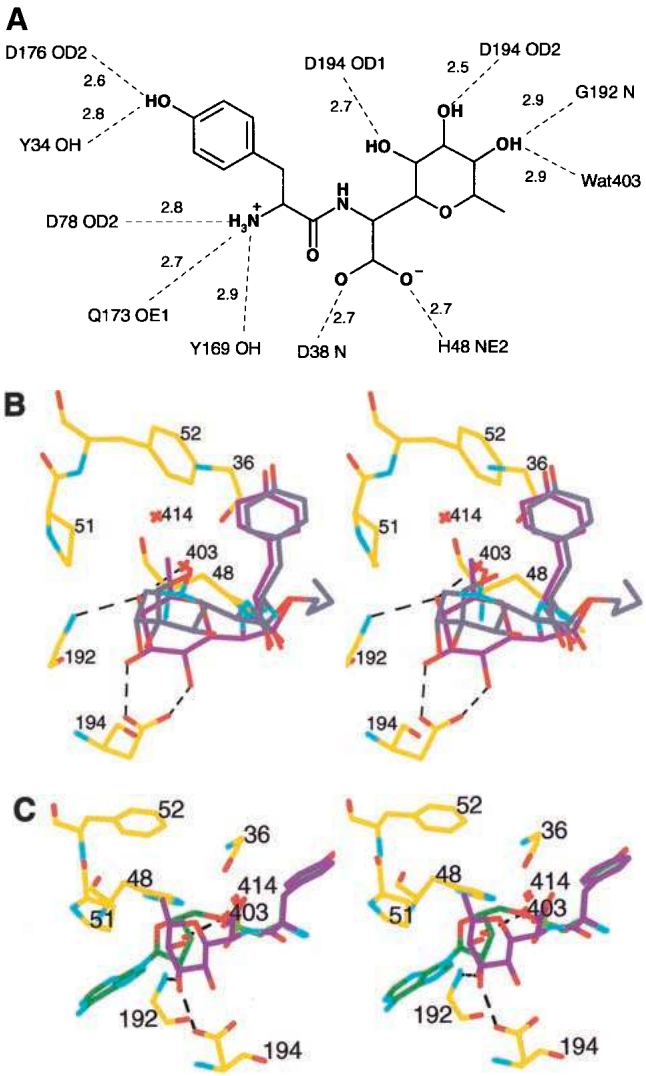

Fig. 7. The binding of SB-284485 to YRS. (*A*) Schematic diagram showing all the hydrogen bonding interactions (dashed lines) between the inhibitor and YRS. The hydrogen bonding distances are labeled. (*B*) Stereoview of the fucose binding mode. Hydrogen bonds are shown in dashed lines. SB-243545 is included for comparison. Protein carbons are in yellow, SB-284485 carbons are in purple, and SB-243545 carbons are in grey. Oxygen is red and nitrogen is cyan. (*C*) Stereoview of the superposition of SB-284485 (purple) and tyrosyl adenylate (green). The latter is shown with ribose hydrogen bonds and is modeled based on bsTyrRS structures.

The amino group is hydrogen bonded to Asp78 OD2 (2.8 Å), Tyr169 OH (2.9 Å), and Gln173 OE1 (2.7 Å), while the hydroxyl is hydrogen bonded to Tyr34 OH (2.8 Å) and Asp176 OD2 (2.6 Å). The tyrosyl carbonyl is 3.4 Å from Asp78 OD2, but forms no hydrogen bonds. The tyrosyl moiety is also involved in van der Waals interactions with YRS residues (e.g. Leu68, Gln173, Gly36, Thr73, Asn123, Gln189, and Gln195). All of these residues are conserved in bsTyrRS (Fig. 2A) and form nearly identical interactions to the tyrosine or tyrosyl in the bsTyrRS structures (Brick et al. 1989). Interestingly, one side of the tyrosyl ring is adjacent to a pair of tightly bound water molecules, Wat403 and Wat414. Wat403 binds to Gly36 O (2.7 Å) and Wat414 (3.0 Å); Wat414 is also within hydrogen bonding distance to Val191 O (2.8 Å), Gly36 N (3.2 Å) and Gln189 OE1 (2.9 Å). Both waters are observed in the same positions in bsTyrRS (Brick et al. 1989). This suggests that bulkier tyrosyl derivatives may fit well into the tyrosine binding pocket of either enzyme by displacing the water molecules.

Unlike the tyrosyl group, the unnatural amino acid in the SB-284485 "dipeptide" is not identical to any part of the TyrRS substrates. Its nitrogen atom is 3.3 Å from Wat403, but does not form any hydrogen bond. The carboxylate oxygen atoms are hydrogen bonded to the main chain nitrogen of Asp38 (2.7 Å), as well as the side chain of His48 (2.7 Å, Fig. 7A). The former hydrogen bond mimics that of a phosphate oxygen in tyrosyl adenylate (Brick et al. 1989), but the latter reaches a little beyond this phosphate and could be similar to one formed with the ATP pyrophosphate. The most interesting component of SB-284485 is probably the fucose ring, which appears to interact really well with YRS (Fig. 7B). While one of its hydroxyls interacts with Gly192 N (2.9 Å) and Wat403 (2.9 Å), another forms a hydrogen bond with Asp194 OD2 (2.5 Å). These two hydroxyl groups imitate nearly perfectly the two ribose hydroxyls in tyrosyl adenylate. The third fucose hydroxyl binds to Asp194 OD1 (2.7 Å), hence gaining an extra hydrogen bond over those present with ribose. The methyl group on the fucose ring, which increases the affinity of the fucose inhibitors by two orders of magnitude compared to their arabinose counterparts (Brown et al. 2001), forms good van der Waals interactions with Phe52 and Pro51. The additional binding elements in the fucose analogue could be the reason for the higher inhibitory potency than seen with the ribose system in the adenylate analogues. The six-member fucose ring actually shows less homology to the six-member monocyclic ring of SB-239629 and SB-243545. In the overlay of the two inhibitor complex structures (Fig. 7B), the fucose ring is almost perpendicular to the monocyclic ring in SB-243545. While the hydrogen bonds to Asp194 are similar, the fucose ring lacks the hydrogen bonds to the His48 side chain and Gly36 O, but gains the hydrogen bonds to Gly192 N and Wat403. The total number of hydrogen bonds is the same for the two ring systems, which may explain their equivalent overall potencies (Fig. 1) despite rather different binding modes.

Implications in inhibitor design

The structures of the YRS-inhibitor complexes provide valuable insights into further inhibitor design. We have mentioned quite a number of binding sites in YRS in this report: tyrosine, α-phosphate, ribose, adenine, butyl and pyrophosphate. All these sites could be the subjects of further exploration for inhibitor design. For example, a bulkier tyrosyl derivative may be designed to displace the water molecules in the tyrosine binding pocket. This is probably more suitable for the fucose ring series (SB-284485) because Wat403 has almost certainly been displaced already by one of the hydroxyl groups in the other series (SB-219383, SB-239629 and SB-243545). Another example is the butyl binding site, which seems to have extra room for additional apolar or even polar interactions (Fig. 7B). Moreover, these inhibitors have used neither the adenine binding site nor the pyrophosphate binding site. Of course, an inhibitor using all the available sites is likely too big to be useful as a drug. However, if potency can be obtained with all these sites, there could be opportunities for mixing and matching the binding components to afford drastic changes in the physical properties of the inhibitors. For example, there could be a need to eliminate the positive charge of the tyrosyl amino group to increase bacterial membrane permeability. It may also become necessary to minimize the peptide characteristics of the inhibitors by modifying the tyrosyl carbonyl group and the peptide nitrogen atom. Except for some plasticity at the HIGH motif, other active site residues do not seem to move that much in the YRS structures. Though there are minor differences near residue 51, most other amino acids in the active sites are well conserved in the two bacterial enzymes. This means broad spectrum antimicrobial agents may be attainable via targeting TyrRS. The sequence identity between human and bacterial TyrRS is less than 20% (Kleeman et al. 1997), suggesting that compounds specific to bacterial TyrRS may be obtained. Because SB-284485 is synthesized more readily, it provided an excellent template for further SAR studies. As one example, the butyl ester derivative of SB-284485 has already been made and is indeed more potent (Brown et al. 2001).

Materials and methods

Protein production and purification

Full-length *Staphylococcus aureus* tyrosyl-tRNA synthetase (YRS) was over-expressed in *E. coli* and purified to homogeneity in four steps: Q Sepharose (eluted using a linear 0–650 mM NaCl gradient), Phenyl Sepharose (2–0 M $(NH_4)_2SO_4$ gradient), and Source 15Q (linear 0–1 M NaCl gradient). Protein samples were assessed by activity assays and SDS-PAGE, and concentrated to 5

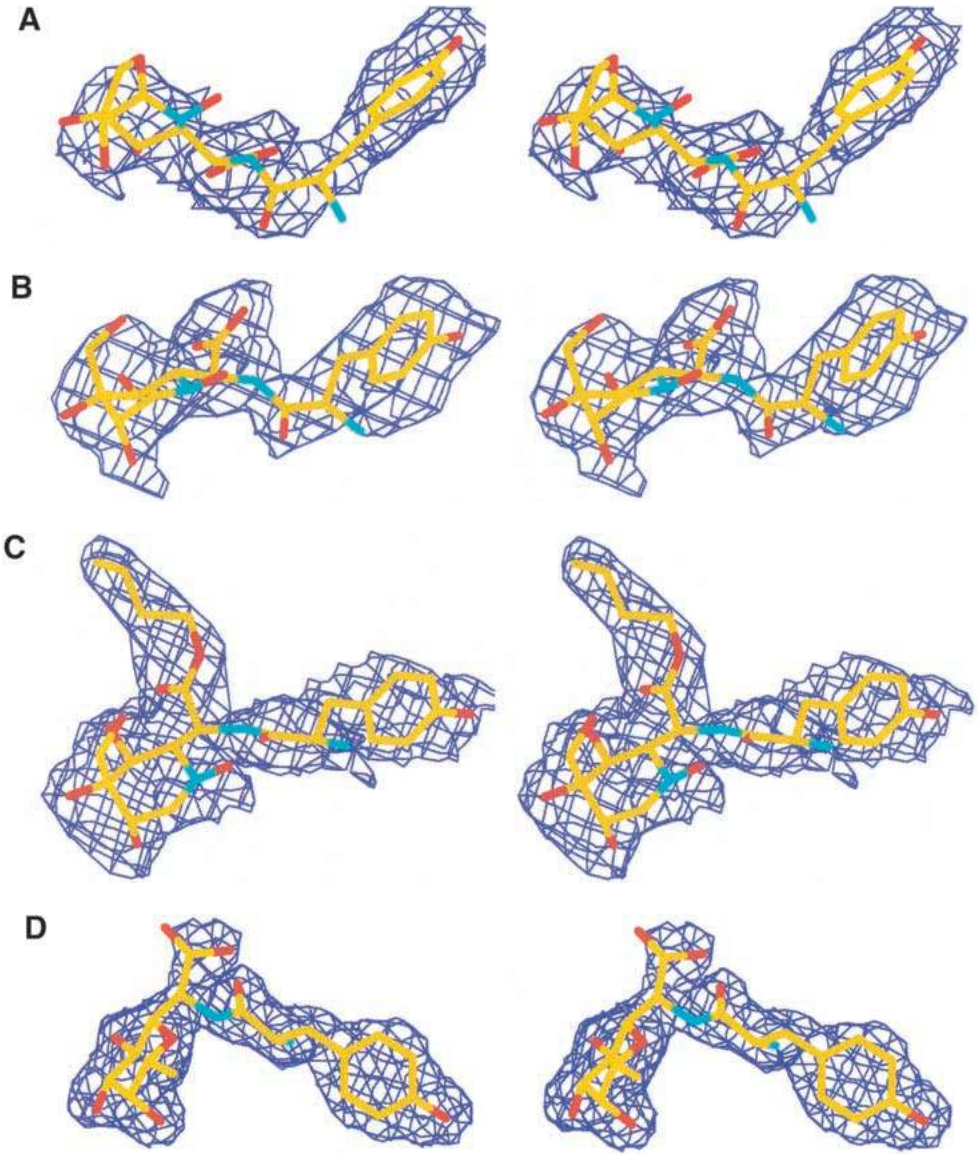

Fig. 8. Stereoviews of the Electron Density (2Fo–Fc) Maps for the YRS Inhibitors. (*A*) The density for SB-219383 contoured at 1 σ. (*B*) The density of SB239629 contoured at 1 σ. (*C*) The density for SB-243545 contoured at 1 σ. (*D*) The density for SB-284485 contoured at 1.5 σ.

mg/mL for crystallization. The YRS truncation was achieved by inserting a stop codon in the original construct, after the DNA sequence encoding Asp326. The truncated protein, YRS^{tr}, is expressed in a manner similar to that of the full length protein. Purification of YRS^{tr} (1–326) was carried out via $(NH_4)_2SO_4$ precipitation, Source 15 Q (0–1 M linear gradient of NaCl) and Source 15 Phenyl (1.2–0 M $(NH_4)_2SO_4$ gradient) steps. The protein sample was concentrated to 10 mg/mL for crystallization trials.

Crystallization and data collection

Details about the preparation of the five chemical compounds have been reported (Berge et al. 2000a; Berge et al. 2000b; Houge-Frydrych et al. 2000; Stefanska et al. 2000; Brown et al. 2001). SB-284485 was supplied as a mixture of the two diastereomers at the unnatural amino acid center and the correct compound (*S* diastereomer, IC_{50} 4 nM) was observed in the crystal. Solid compound was mixed with the purified YRS protein (10mg/mL) and incubated for two days before crystallization trials. The crystals were grown using sitting-drop vapor diffusion methods. The well solution contained 12–15% PEG 1000, 0.15 M $CaCl_2$ and 0.2 M imidazole buffer at pH 7.25. The drop solution was a mixture of protein and well solutions in a 1:1 ratio. Crystals appeared in three to seven days, often at a size of 0.2 mm × 0.2 mm × 0.6 mm. Diffraction data on the YRS383, YRS629, and YRS545 crystals (Table 1) were collected in house at room temperature using a Siemens area detector. Data of the YRS^{tr}485 crystal (Table 1) were obtained at cryogenic temperatures on the beamline 12-B at the National Synchrotron Light Source of the Brookhaven National Laboratory. Details of all the data sets are listed in Table 1. There are two different crystal forms for these structures, $C222_1$ and

$I2_12_12_1$. In both crystal forms, there is one YRS monomer per asymmetric unit.

Structure solution and refinement

The amino acid sequence of YRS is about 61% identical to that of bsTyrRS. The crystal structure of YRS383 was solved by the method of molecular replacement using the program XPLOR (Brunger 1987). The crystal structure of bsTyrRS was used to construct a search model, which included all the side chain atoms of conserved amino acids and alanines where the two TyrRS sequences differ. Using data from 8.0 to 4.0 Å resolution, the rotation search yielded a clear solution that is 22σ in peak height, 3.5σ higher than the second highest peak. The translation solution gave a 20σ peak and a 46.7% R factor (10.0–3.2 Å). The latter was further reduced to 45.3% after 40 cycles of rigid body refinement. Upon further phase modification using solvent flattening and histogram matching procedures, the electron density map was interpretable. Five percent of the data was set aside for free-R validation. Iterations of manual model building using XTALVIEW (McRee 1993) and refinement using XPLOR led to the final structure, which has an R_{cryst} of 26.9% and R_{free} of 33.5% (8.0–3.2 Å). An overall B-factor is used during the structural refinement. The partial disordering of the 100 residue C-terminal domain may be the cause of this relatively large difference between R_{cryst} and R_{free}. Because its unit cell is similar to that of YRS383, the YRS629 structure (Table 1) was solved by difference Fourier methods. Model building and refinement procedures are as just described for YRS383 (Table 1). The YRS545 crystal diffracted to 2.8 Å resolution, which is a notable improvement in data quality. The structure of YRS545 was solved by molecular replacement methods, this time using the YRS383 structure as the search model. The structure has been refined with individual atomic B-factors. The monocyclic ring in this structure superimposes nearly perfectly onto that of SB-239629, which supports the validity of the two structures determined at 3.2 Å resolution. All three structures of the full-length YRS enzyme, although somewhat limited by the diffraction resolution, are of better quality than average structures determined at the same resolutions (Table 1) and adequate for observing the binding modes of these inhibitors (Fig. 8).

Similar to that of bsTyrRS, the C-terminal domain of YRS is disordered in the crystals. This domain is truncated in our YRS^{tr} protein, which binds our inhibitors with similar potencies and catalyzes tyrosine adenylation competently, but is not expected to bind $tRNA^{tyr}$. For bsTyrRS, such a truncation did not yield crystals of better diffraction (Brick and Blow 1987). However, the crystal of YRS^{tr} in complex with SB-284485 (YRS^{tr}485) diffracts to at least 2.2 Å resolution, which is a significant improvement over the crystals of our full-length YRS protein. The YRS^{tr}485 structure was solved using the YRS545 model and rigid-body refinement. The structure has been refined using the newer program CNX (Brunger et al. 1998) and all the data from 45.0 to 2.2 Å resolution. Solvent molecules were clearly visible at this resolution and therefore were included in the structural model. The final R_{cryst} is only 18.3% (R_{free} 22.1%). Not a single residue is in the generously allowed or disallowed regions of the Ramachandran plot. The YRS^{tr}485 structure is of excellent quality and is used for the general description of the YRS structure. Coordinates of our structures have been deposited in Protein Data Bank, with access codes 1JII, 1JIJ, 1JIK and 1JIL.

Acknowledgments

We thank the NSLS X12B staff at Brookhaven National Laboratory for their assistance in data collection. We also appreciate the support from Drs. Andy Pope, Christine Richardson, Ben Bax, Sherin Abdel-Meguid, Peter O'Hanlon and Drake Eggleston.

The publication costs of this article were defrayed in part by payment of page charges. This article must therefore be hereby marked "advertisement" in accordance with 18 USC section 1734 solely to indicate this fact.

References

Berge, J.M., Copley, R.C., Eggleston, D.S., Hamprecht, D.W., Jarvest, R.L., Mensah, L.M., O'Hanlon, P.J., and Pope, A.J. 2000a. Inhibitors of bacterial tyrosyl tRNA synthetase: Synthesis of four stereoisomeric analogues of the natural product SB-219383. *Bioorg. Med. Chem. Lett.* **10:** 1811–1814.

Berge, J.M., Broom, N.J.P., Houge-Frydrych, C.S.V., Jarvest, R.L., Mensah, L.M., McNair, D.J., O'Hanlon, P.J., Pope, A.J., and Rittenhouse, S. 2000b. Synthesis and activity of analogues of SB-219383: Novel potent inhibitors of bacterial tyrosyl tRNA synthetase. *J. Antibiot. (Tokyo)* **53:** 1282–1292.

Brick, P. and Blow, D.M. 1987. Crystal structure of a deletion mutant of a tyrosyl-tRNA synthetase complexed with tyrosine. *J. Mol. Biol.* **194:** 287–297.

Brick, P., Bhat, T.N., and Blow, D.M. 1989. Structure of tyrosyl-tRNA synthetase refined at 2.3 Å resolution. Interaction of the enzyme with the tyrosyl adenylate intermediate. *J. Mol. Biol.* **208:** 83–98.

Brown, K.A., Brick, P., and Blow, D.M. 1987. Structure of a mutant of tyrosyl-tRNA synthetase with enhanced catalytic properties. *Nature* **326:** 416–418.

Brown, P., Berge, J.M., Hamprecht, D.W., Jarvest, R.L., McNair, D.J., Mensah, L., O'Hanlon, R.J., and Pope, A.J. 2001. Synthetic analogues of SB-219383. Novel C-glycosyl peptides as inhibitors of tyrosyl tRNA synthetase. *Bioorg. Med. Chem. Lett.* **11:** 715–718.

Brown, P., Richardson, C.M., Mensah, L.M., O'Hanlon, P.J., Osborne, N.F., Pope, A.J., and Walker, G. 1999. Molecular recognition of tyrosinyl adenylate analogues by prokaryotic tyrosyl tRNA synthetases. *Bioorg. Med. Chem.* **7:** 2473–2485.

Brunger, A.T. 1987. *X-PLOR version 3.1, A system for X-ray crystallography and NMR.* Yale University Press, New Haven, CT.

Brunger AT, Adams PD, Clore GM, DeLano WL, Gros P, Grosse-Kunstleve RW, Jiang JS, Kuszewski J, Nilges M, Pannu NS, et al. 1998. Crystallography & NMR system: A new software suite for macromolecular structure determination. *Acta Crystallogr.* **D54:** 905–921.

Eriani, G., Delarue, M., Poch, O., Gongloff, J., and Moras D. 1990. Partition of tRNA synthetases into two classes based on mutually exclusive sets of sequence motifs. *Nature* **347:** 203–206.

Fersht, A.R. 1975. Demonstration of two active sites on a monomeric aminoacyl-tRNA synthetase. Possible roles of negative cooperativity and half-of-the-sites reactivity in oligomeric enzymes. *Biochemistry* **14:** 5–12.

Fersht, A.R. 1985. *Enzyme Structure and Function*. Freeman and Co., New York.

Fersht, A.R., Knill-Jones, J.W., Bedouelle, H., and Winter G. 1988. Reconstruction by site-directed mutagenesis of the transition state for the activation of tyrosine by the tyrosyl-tRNA synthetase: A mobile loop envelopes the transition state in an induced-fit mechanism. *Biochemistry* **27:** 1581–1587.

Houge-Frydrych, C.S.V., Readshaw, S.A., Bell, D.J. 2000. SB-219383, a novel tyrosyl tRNA synthetase inhibitor from a *Micromonospora* sp. II. Structure determination. *J. Antibiot. (Tokyo)* **53:** 351–356.

Hudson, I.R. 1994. The efficacy of intranasal mupirocin in the prevention of staphylococcal infections: A review of recent experience. *J. Hosp. Infect.* **27:** 81–98.

Kleeman, T.A., Wei, D., Simpson, K.L., and First, E.A. 1997. Human tyrosyl-tRNA synthetase shares amino acid sequence homology with a putative cytokine. *J. Biol. Chem.* **272:** 14420–14425.

Leatherbarrow, R.J., Fersht, A.R., and Winter, G. 1985. Transition-state stabilization in the mechanism of tyrosyl-tRNA synthetase revealed by protein engineering. *Proc. Natl. Acad. Sci. USA* **82:** 7840–7844.

McRee, D.E. 1993. *Practical Protein Crystallography*. Academic Press, New York.

Reid, B.R., Koch, G.L., Boulanger, Y., Hartley, B.S., and Blow, D.M. 1973. Crystallization and preliminary X-ray diffraction studies on tyrosyl-transfer RNA synthetase from *Bacillus stearothermophilus*. *J. Mol. Biol.*. **80:** 199–201.

Schimmel, P., Tao, J., and Hill, J. 1998. Aminoacyl tRNA synthetases as targets for new anti-infectives. *FASEB J.* **12:** 1599–1609.

Stefanska, A.L., Coates, N.J., Mensah, L.M., Pope, A.J., Ready, S.J., and Warr, S.R. 2000. SB-219383, a novel tyrosyl tRNA synthetase inhibitor from a *Micromonospora sp*. I. Fermentation, isolation and properties. *J. Antibiot. (Tokyo)* **53:** 345–350.